# Cinnamaldehyde hydrogenation using Au-Pd catalysts prepared by sol immobilisation

*Stefano Cattaneo, Simon J. Freakley, David J. Morgan, Meenakshisundaram Sankar, Nikolaos Dimitratos, and Graham J. Hutchings*[*]

*Cardiff Catalysis Institute, School of Chemistry, Cardiff University, Cardiff, CF10 3AT, United Kingdom.*

* Hutch@cardiff.ac.uk

**Abstract**

We report the catalytic performance of Au-Pd nanoparticles prepared via a sol immobilisation technique for the catalytic hydrogenation of cinnamaldehyde under mild reaction conditions. We synthesised a series of bimetallic Au-Pd colloidal supported nanoparticles with different Au:Pd molar ratios and optimized the experimental parameters to achieve best catalyst performance. The optimum catalytic activity for the hydrogenation of cinnamaldehyde was observed for the $Au_{50}Pd_{50}/TiO_2$ (Au:Pd 1:1 molar ratio), while the monometallic $Pd/TiO_2$ was the most selective towards hydrocinnamaldehyde. The catalysts have been structurally characterised and FTIR analysis showed that the presence of adsorbed carbonyl surface species in used catalyst materials coupled with Pd leaching, which is the main reason for catalyst deactivation. The effect of calcination on the most active $Au\text{-}Pd/TiO_2$ was studied in the range 110-400 °C and we observed a direct correlation between the rise in calcination temperature and catalyst stability and selectivity. These results emphasise the importance of tuning the Au-Pd molar ratio and understanding the metal-support interaction of catalysts synthesised for hydrogenation reactions, such as cinnamaldehyde hydrogenation.

## Introduction

Supported palladium nanoparticles based catalysts are widely reported as heterogeneous catalysts for many organic transformations such as selective alcohol oxidation,[1] unsaturated hydrocarbon hydrogenation,[2] and C-C coupling reactions.[3] It has been shown that alloying palladium with gold enhances its catalytic activity for the oxidation of benzyl alcohol[4] hydrogenation of levulinic acid to *gamma*-valerolactone[5] and the direct synthesis of hydrogen peroxide,[6] demonstrating a synergistic in both oxidation and hydrogenation reactions. α,β-unsaturated aldehydes are important molecules in the pharmaceutical, fragrance and fine chemical industry;[7,8] cinnamaldehyde (CAL) is used extensively in the fragrance industry and also as a polymerisation and corrosion inhibitor in metal coatings.[9,10] The selective hydrogenation of the vinyl (C=C) or carbonyl (C=O) groups of CAL lead to hydrocinnamaldehyde (HCAL) and cinnamyl alcohol (COH) respectively, that are useful intermediates in pharmaceuticals and perfumery.[9,11] Further hydrogenation of the products, results in hydrocinnamyl alcohol (HCOH) and phenyl propane (PPR) by hydrogenolysis (Figure 1). Several transition and noble metal based catalysts are reported in literature to be active in the hydrogenation of cinnamaldehyde.[7] Gold nanoparticles typically require harsh reaction conditions to obtain high conversion and selectively hydrogenate the carbonyl group leading to the formation of COH. *Bus et al.,* reported the conversion of CAL with Au/γ-$Al_2O_3$ to COH with a selectivity up to 90 % at 85 bar of $H_2$ and 100 °C. In their studies, high selectivity to COH were produced from the initial stages of the reaction, and the selectivity remained unaltered up to 85 % of conversion, after which all the COH was further hydrogenated into HCOH.[12] Similar results were obtained by other research groups for Au nanoparticles supported on different supports such as $CeO_2$[13] and α-$Fe_2O_3$.[14] Au supported on CNT, $SiO_2$ and $ZrO_2$, however, has been reported to selectively hydrogenated the C=C bond.[15,16] On the other hand, Pd nanoparticles are more selective towards the hydrogenation of the C=C bond both when supported[17] or stabilised in ionic liquids.[18]

Numerous studies on the effect of support materials, solvents and hydrogen sources have been reported in literature.[12–16,19,20] However, very few articles have been focused on supported AuPd catalysts. Dash *et al.* reported equimolar production of HCAL and HCOH using bimetallic AuPd nanoparticles stabilised in imidazolium ionic liquids when the Au/Pd molar ratio was 3:1 and 1:3. However, the selectivity of HCOH increased substantially for the 1:1 AuPd catalyst.[21] Similar results were reported for the AuPd/C catalysts prepared by reverse water-in-oil microemulsion method.[22] On the other hand, Parvulescu *et al.* observed an

increase in COH production using AuPd colloids embedded in $SiO_2$[23] . Very high selectivity towards HCAL was obtained by Yang *et al.* with bimetallic nanoparticles supported on mesoporous $SiO_2$.[24]

In the present work, pre-formed colloidal AuPd nanoparticles with narrow particle size distribution were prepared *via* a sol-immobilisation method. These pre-formed nanoparticles were then immobilised onto titanium dioxide and tested for the selective hydrogenation of cinnamaldehyde under relatively mild reaction conditions. In this extensive study we report the effect of reaction temperature, hydrogen partial pressure, solvent and Au/Pd molar ratio has been on the catalytic activity, selectivity and the stability of the sol-immobilised catalyst. Finally, an efficient 2-step heat treatment protocol is reported to increase the metal-support interaction, which is crucial for increased activity, selectivity and stability for this selective hydrogenation reaction.

## Experimental

### Materials

$HAuCl_4$ and $PdCl_2$ (99.999 % purity, Sigma-Aldrich) were used as metal precursors and, commercial $TiO_2$ (Degussa, P25) was used as the support. $NaBH_4$ (granular, 99.99 % purity, Sigma-Aldrich) and polyvinyl alcohol (PVA, Mw = 9,000-10,000, 80 % hydrolysed, Sigma-Aldrich) were used for the catalyst preparation. Cinnamaldehyde (Sigma-Aldrich, 99 %), cinnamyl alcohol (Alfa Aesar, 95 %), hydrocinnamaldehyde (Sigma-Aldrich, 98 %), hydrocinnamyl alcohol (Sigma-Aldrich, 98%) and phenylpropane (Sigma-Aldrich, 98 %) were used as substrates and/or as standards. Toluene (Sigma-Aldrich, > 99 %), ethanol (VWR, 99.8 %) and 2-propanol (Sigma-Aldrich, 99.5 %) were used as solvents.

### Catalyst preparation

Sol-immobilisation catalysts were prepared as follows: To an aqueous solution of $HAuCl_4$ and/or $PdCl_2$ of the desired concentration (total metal concentration 0.127, 0.130, 0.143, 0.165, 0.194, and 0.235 mmol/L for Au/Pd molar ratios of 100:0, 95:5, 75:25, 50:50, 25:75 and 0:100 respectively), PVA solution (1 wt %) was added (PVA/(Au + Pd) (w/w) = 1.2 for bimetallic catalysts, 0.65 for monometallic catalysts) under constant stirring. A freshly prepared aqueous solution of $NaBH_4$ (0.1 M, $NaBH_4$/(Au + Pd) (mol/mol) = 5) was then added to form a ruby-red sol when monometallic gold was prepared or a dark-brown sol when AuPd

or Pd sols were prepared. After 30 minutes of sol generation, the colloid was immobilised by adding the $TiO_2$ and acidified at pH 1 by sulfuric acid under continuous vigorous stirring. The amount of support material required was calculated so as to have a total final metal loading of 1 wt. %, and the molar ratio of Au/Pd was varied by adjusting the relative concentrations of the two metals in aqueous solution. After 1 h of stirring, the slurry was filtered and the catalyst was washed thoroughly with 2 L of distilled water and dried at 120 °C for 16 h. Unless specified this dried catalysts were used without any further treatment. In some cases, the dried catalyst was first calcined in static air for 4 hours at either 200, 300 and 400 °C with a heating rate of 10 °C/min and finally reduced at the same heat treatment temperature under a 5 % $H_2$/Ar flow for another 4 hours.

**Catalyst testing**

The hydrogenation reactions were carried out in a Radleys carousel reactor using 5 parallel 50 mL glass reactors stirred using magnetic bars. In a typical reaction, catalyst (50 mg, typical substrate/metal molar ratio 1200:1), substrate (500 µL, 4 mmol) and solvent (5 mL of toluene, ethanol or 2-propanol) were charged into the reactors at room temperature, which were then purged with $H_2$ (3 times) before the reactors were sealed. The reactors were connected to the gas-line to replenish the consumed $H_2$ gas. The reactors were loaded into a preheated heating block, which was maintained at the desired reaction temperature and pressure (typically 100 °C and 1 $H_2$ bar). The reaction started by commencing stirring inside the reactors at 1000 rpm. After the desired reaction time, the reactors were taken out the carousel and cooled down in an ice bath for a period of 5 minutes to quench the reaction. The contents were then centrifuged and an aliquot of the clear supernatant reaction mixture (0.5 mL) was diluted with an external standard (0.5 mL of a 0.7 M solution of o-xylene in the appropriate solvent) for GC measurement. For the analysis of the products, a GC-MS (Shimadzu, GCMS-QP2010SE) was employed and the resulting fragmentation peaks compared with standards present in the software database, while for the quantification of the amounts of reactants consumed and products generated, a GC-FID (Agilent 7820A equipped with an Agilent HP-5, 30 m x 320 µm x 0.25 µm column) was employed and the external calibration method was used. Turnover frequency (TOF) were calculated according to the following equation:

$$TOF = \frac{mol_{conv}}{mol_{Me} * t}$$

where $mol_{conv}$ is the moles of CAL converted, $mol_{Me}$ is the moles of the active sites and t is the reaction time in hours. The total metal content was obtained from MP-AES analysis.

The catalyst reusability was carried out using the following experimental procedure. After 90 minutes of reaction, the flask was cooled to room temperature in an ice bath and the catalyst allowed to settle at the bottom of the flask. The supernatant liquid reaction mixture was removed carefully and the solid catalyst was washed with acetone 2 times and allowed to dry in air. A second reaction was then started with the washed catalyst and this procedure was repeated 4 times.

**Catalyst characterisation**

The metal colloids were analysed by UV-Vis (Agilent Cary 60) spectroscopy to study the surface plasmon resonance peak of gold and the completion of metal reduction. The UV-vis spectra were recorded in quartz cuvettes after 30 minutes of sol generation.

TEM experiments were carried out on a JEOL JEM-2100 electron microscope with a 200 kV accelerating voltage. The samples were first dispersed in methanol and sonicated for 5 minutes and then a drop was placed onto a 300 mesh carbon-coated copper grid.

Nitrogen physisorption analysis was performed at – 196 °C with a Quantachrome Quadrasorb SI after evacuation of the samples at 120 °C for 2 hours. Surface area and pore volume were calculated using Brunauer-Emmet-Teller (BET) theory.

Powder XRD measurements were carried out at room temperature in a PANalytical X'PertPRO instrument using a Cu Kα radiation source, (Kα, λ= 1.5418 A$^{o}$). The diffractograms were collected over the 10-80 ° 2θ range at a rate of 1 °/min. The metal loading of the catalysts was verified using an Agilent 4100 MP-AES. The samples were firstly dissolved in aqua regia, diluted and filtered to remove the undissolved support. X-ray photoelectron spectroscopy (XPS) measurements were performed on a Thermo Scientific K-alpha+ spectrometer. Samples were analysed using a monochromatic Al X-ray source operating at 72 W (6 mA x 12 kV), with the signal averaged over an oval-shaped area of approximately 600 x 400 microns. Data was recorded at pass energies of 150 eV for survey scans and 40 eV for high resolution scan with a 1eV and 0.1 eV step size respectively. Charge neutralisation of the sample was achieved using a combination of both low energy electrons and argon ions (less than 1 eV) which gave a C(1s) binding energy of 284.8 eV. All data were analysed using CasaXPS (v2.3.17 PR1.1) using Scofield sensitivity factors and an energy exponent of -0.6.

Diffuse reflection infrared spectroscopy (DRIFTS) was carried out with a Bruker Tensor 27 spectrometer fitted with a HgCdTe (MCT) detector and operated with OPUS software. The Harrick Praying Mantis HVC-DRP-4 cell was equipped with ZnSe windows and included gas

inlet and outlet and vacuum ports as well as capabilities for heating and cooling. The required gas flow was introduced using a 2 % $CO/N_2$ gas mixture at 40 $cm^3$ $min^{-1}$ of, over a period of 60 minutes. The mixture composition and flow rate was controlled by mass-flow controllers. Each absorbance spectrum represents an average of 64 scans with a spectral resolution of 2 $cm^{-1}$. Prior to analysis, the gas-phase CO signal was removed by subtracting the spectra recorded under CO containing atmosphere, followed by background and normalisation of the spectra. No high temperature pretreatments were performed on the catalysts in order to avoid sintering of metal nanoparticles.

## Results and discussion

### Catalyst characterisation

A series of AuPd catalysts with varying metal ratios were prepared. The AuPd metal loading and ratios were confirmed by XPS & MP-AES (total metal content = 1 wt. %) (Supporting information, Table S1). The average metal particle size and particle size distribution of the catalysts were determined by TEM (supporting information, Figure S1 and Table S2). Representative bright field TEM micrographs of monometallic and bimetallic catalysts are presented in Figure 2. The mean particle sizes of all the supported bimetallic $Au_xPd_y$ nanoparticles were between 2.1 (±0.4) - 2.7 (± 1.0) nm without any appreciable size variation for different AuPd ratios. The presence of small metal nanoparticles was evidenced by the low intensity of Au (200) and Pd (200) reflexions in the powder XRD of the catalysts (supporting information, Figure S2). BET analysis on the bare support $TiO_2$ and on the final $Au_{50}Pd_{50}/TiO_2$ shows no substantial difference in surface area and porosity due to metal deposition (Table S3).

XPS data of the supported monometallic and bimetallic catalysts are presented in Figure 3. For the whole series of samples, the $Au4f_{7/2}$ peak were between 83.3-83.7 eV confirming that Au is in the metallic state.[25] The Pd(3d) spectra showed the presence of metallic Pd (334.9 eV) as the major species and some $Pd^{2+}$, attributed to PdO (337.0 eV) since no chloride is detected, (Figure 3). For the monometallic $Au/TiO_2$ sample the B.E. of Au was 83.7 eV, lower than that of bulk gold (*ca.* 84.0-84.2 eV). This slight decrease in B.E. is be attributed to (i) particle size effects and (ii) charging of Au particles (presence of Au with partially negative charge $Au^{\delta-}$). The addition of Pd to the Au samples caused a downward shift in the BE of Au from 83.7 to 83.3 eV indicating an electronic interaction between the Au and Pd as noted by

Lee *et al.* [26] In common with that study the Pd B.E. shifts were no greater than 0.2 eV, which we consider to be the experimental confidence limit for absolute B.E. (supporting information, Figure S3). With the small size of the nanoparticles, the photoelectron attenuation lengths are of the same order as the particle sizes, therefore absolute information on the formation of core-shell particles from XPS alone is difficult, however analysis of the bimetallic catalysts revealed the Pd/Au atomic ratios were close to the expected nominal values suggesting the presence of random alloys rather than core-shell structures and in agreement with our previous reports (supporting information, Table S1)[27].

CO-DRIFTS analysis was performed on the bimetallic Au-Pd and monometallic Au, Pd nanoparticles supported on $TiO_2$, Figure 4. The monometallic Au catalyst shows a primary peak at around 2120 $cm^{-1}$ comprised of two peaks at 2124 and 2112 $cm^{-1}$ assigned to CO linearly bonded on $Au^0$ step sites on top of nanoparticles and on peripheral $Au^0$ step sites respectively (deconvolution shown in supporting information, Figure S4).[28] The presence of the latter peak, in particular, suggests the presence of small nanoparticles on the catalyst surface. The peak at 2072 $cm^{-1}$, on the other hand, has been assigned to linear CO adsorbed on $Au^{\delta-}$ species.[29] These partially negative species form during the gradual reduction of $Au^0$ to $Au^{\delta-}$ by the adsorbed CO at high CO partial pressure,[30] as shown by comparison of the spectra at low CO partial pressure (supporting information, Figure S4). The broad peak at 2050-1950 $cm^{-1}$ has been assigned to bridge bonded CO on $Au^{\delta-}$ species. The presence of this broad band is a direct effect of very well dispersed small Au nanoparticles on the surface of support, as reported by *Tabakova et al.*[31]

The CO-DRIFTS spectra of monometallic Pd catalyst (deconvolution shown in supporting information, Figure S5), consists of two broad groups of peaks. The first group, is comprised of 3 peaks at 2130, 2096 and 2083 $cm^{-1}$; the latter two peaks have been assigned to linear CO coordinated on $Pd^0$,[32–34] while the peak at 2130 $cm^{-1}$ suggests the presence of cationic Pd species,[33,34] most likely PdO, in agreement with XPS analysis. The second group at lower wavenumbers, is comprised by multiple and broad peaks assigned to $\mu_2$ bridge bonded CO (ca. 1980-1930 $cm^{-1}$) and $\mu_3$ bridge bonded CO (ca. 1930-1820 $cm^{-1}$) in accordance with previous literature.[32,34]

In the case of bimetallic AuPd catalysts, it has been previously reported that Pd carbonyls are much more stable than Au carbonyls due to the higher π-back-donation of the Pd-CO bond.[35]

For this reason, the typical Pd-CO bands dominate the DRIFTS spectra in AuPd alloys when Pd is present in significant amount and it is therefore difficult to observe bands related to the presence of Au sites. Indeed, for the $Au_{35}Pd_{65}$, $Au_{50}Pd_{50}$ and $Au_{65}Pd_{35}$ catalysts, all the CO-Pd features observed for the monometallic Pd catalyst are present,[36] with varying intensities corresponding to the amount of Pd (supporting information, Figure S6). The same explanation applies to the $Au_{65}Pd_{35}$ catalyst, where the nanoparticle mean size is very similar to the $Pd/TiO_2$. Interestingly, when the Au/Pd ratio is 95:5, the CO stretching modes are dominated by the CO-Au interactions (supporting information, Figure S7). The appearance of a strong peak at 2123 $cm^{-1}$ with a small shoulder at 2103 $cm^{-1}$ is evident and these peaks are characteristic of linear CO bonded on $Au^0$ step sites on top of nanoparticles and of peripheral $Au^0$ step sites.

**Cinnamaldehyde hydrogenation over $Au_{50}Pd_{50}/TiO_2$**

Cinnamaldehyde (CAL) hydrogenation reactions were initially performed at 100 °C and under 1 bar of $H_2$ using a bimetallic gold-palladium catalyst ($Au_{50}Pd_{50}/TiO_2$, 1 wt.%, 1:1 Au/Pd molar ratio) as our chosen model catalyst, and the main products observed were cinnamyl alcohol (COH), hydrocinnamaldehyde (HCAL), hydrocinnamyl alcohol (HCOH) and phenylpropane (PPR) (Figure 5). The conditions to avoid diffusion limitations were identified to ensure reactions were not under mass transfer limitations (supporting informations, Figure S8).

The influence of hydrogen pressure on both activity and selectivity was also investigated. Several experiments were carried out varying the hydrogen pressure from 1 to 3 bar and using the optimised reaction conditions reported above. The increase of $H_2$ pressure enhances the concentration of the gas in the reaction medium, increasing the accessibility of the $H_2$ molecule. Figure 6a shows that the TOF for cinnamaldehyde hydrogenation increased linearly from 600 to 1080 $h^{-1}$ as the partial pressure increased in the studied range, confirming that the reaction is a first order in respect of the hydrogen partial pressure.[24] The reaction temperature effect was subsequently evaluated by varying the reaction temperature from 40 to 100 °C and maintaining the hydrogen partial pressure constant at 1 bar. It is well known that hydrogenation rates usually increase with increasing temperatures,[7] and here too there is a direct correlation between TOF and temperature (Figure 6b). It should be noted, however, that the hydrogenation selectivity to HCAL at iso-conversion level over the $Au_{50}Pd_{50}/TiO_2$ catalyst remained unchanged with variation of both $H_2$ pressure and reaction temperature (supporting

information, Figure S9 c and d, 40 – 45 % selectivity at 30 % of iso-conversion). This behaviour is in agreement with previous studies on bimetallic catalysts.[24,37,38] The apparent activation energy, from Arrhenius plot, was 24 kJ $mol^{-1}$ (supporting information, Figure S10). The obtained value is in good agreement with the data reported in the literature for various metal based catalysts (supporting information, Table S4).[38–42]

### 3.4 Solvent effects

Toluene was initially employed as solvent in order to avoid potential transfer hydrogenations of CAL with hydrogen donor solvents.It has been shown previously that the solvent plays a very important role in this reaction in terms of activity and selectivity.[12,14,19,22,23]. Besides toluene, polar solvents (ethanol and isopropanol) were also tested for the hydrogenation of cinnamaldehyde hydrogenation. It has been reported for the CAL hydrogenation reaction over Pd/C, Pt/C and $Co/Al_2O_3$, that polar solvents promote the hydrogenation of carbonyl group, while non-polar solvents favour the hydrogenation of the vinyl group.[43] Our results (Figure 7) show a small variation of catalytic activity (± 7 % conversion after 2 hours), between the three solvents studied, however significant difference in selectivity is observed between the solvents. It is interesting to notice the strong decrease in selectivity to HCAL, with ethanol (only 3 % is produced at 85 % conversion), and the increase of PPR selectivity (from 3 % with toluene up to 18 % with ethanol). In presence of Lewis acid sites and small chain alcohols, it has been previously reported for this reaction the formation of acetals.[14,23] Indeed, when both ethanol and isopropanol were used, considerable amounts of acetals were produced (33 % and 25 % respectively).

### 3.5 Effect of Au/Pd molar ratio

The effect of Au/Pd molar ratio on (i) cinnamaldehyde hydrogenation activity (adsorption of cinnamaldehyde on metal active sites) and (ii) the selectivity towards to the C=O or C=C hydrogenation was studied. A series of catalysts with different Au/Pd metal molar ratios were prepared (Au, $Au_{95}Pd_5$, $Au_{65}Pd_{35}$, $Au_{50}Pd_{50}$, $Au_{35}Pd_{65}$, and Pd, supporting information, Table S1). Monometallic $Au/TiO_2$ and $Au_{95}Pd_5/TiO_2$ catalysts were inactive (Figure 8); an increase of catalytic activity based on TOF was observed only with a further addition of Pd, meaning that a minimum amount of this noble metal is required to initiate the reaction. This is in agreement with the CO-DRIFT results (Figure 4), where no Pd features were detected in the $Au_{95}Pd_5$ catalyst. When the molar ratio between Au and Pd is approximately 50:50, the activity reached a maximum with a TOF of 836 $h^{-1}$, and a further addition of Pd decreased the catalytic performance. Activity enhancement due to alloying effect were also reported by other

groups, but no effect on selectivity was reported.[21,24] Only *Parvulescu et al.*, reported an increase in COH selectivity using AuPd colloid embedded in $SiO_2$ as catalyst,[23] while Szumelda and co-workers observed a progressive decrease in both activity and selectivity towards HCAL starting from a Pd/C catalyst and increasing the amount of Au.[22] In both cases, changes in selectivity are explained as geometric and electronic effects. It is clear from these results that Au, although totally inactive when is present alone under our experimental conditions, plays an important role when alloyed with Pd, increasing the catalytic activity of more than 50 % with respect to the monometallic Pd (from 541 to 836 $h^{-1}$). In terms of selectivity, contrary of what previously reported by Parvulescu and co-workers for AuPd on $SiO_2$, an increase in the content of Pd leads to higher production of HCAL up to 82 % in selectivity, with a consequential decrease in HCOH selectivity at iso-conversion levels (Figure 9). It is possible that this selectivity improvement is simply caused by the increase in Pd availability on the surface of the nanoparticles with the increase of total Pd content.

### 3.6 Catalyst stability

$Au_{50}Pd_{50}/TiO_2$ catalyst was tested in multiple consecutive reactions in order to evaluate its reusability. The results are reported in Figure 10. After the first run, the conversion decreased from 73 % to 50 % and it stabilised at a value of 45 % for the following runs. The selectivity, however, changed accordingly to the conversion level (HCOH decreased from 56 % to 45 %), indicating that the deactivation process affects mainly the catalytic activity rather than the selectivity. MP-AES analysis showed a significant loss (about 22 %) of the Pd content after 4 runs that partially explain the loss in activity. Pd leaching was also detected when the reaction was performed with the monometallic $Pd/TiO_2$ catalyst, with a 28 % loss after 4 consecutive reactions. A control experiment using the hot filtrate solution without catalyst confirmed that eventual leached species do not take active part to the reaction. Sintering of metal nanoparticles could be another reason for catalyst deactivation. TEM analysis of the spent catalyst (Table 1) showed an increase in the mean particle size as well as a broadening in size distribution. The FTIR spectra of the fresh and spent catalysts (supporting information, Figure S11), show a weak band at 1670 $cm^{-1}$ accompanied by a broad band in the range of 3700-3000 $cm^{-1}$ that can be attributed to the OH stretching and bending typical for the stabilising agent used (supporting information, Figure S12). However, the enhanced peak at 1670 $cm^{-1}$ in the spent catalyst can be also attributed to the alcoholic functional group of the CAL hydrogenation products and a series of small peaks at around 1500-1400 $cm^{-1}$ typical account for the presence of aromatic C=C stretches that indicate the presence of either COH or HCOH

adsorbed on the surface of the catalyst (supporting information, Figure S13). The stronger band at 3700-3000 $cm^{-1}$ in the fresh catalyst is only due to remaining adsorbed water on the catalyst surface.

In order to improve the catalyst reusability, the $Au_{50}Pd_{50}/TiO_2$ catalyst was heated at 200, 300 and 400 °C. High temperature calcination/reduction steps improve the metal-support interaction *via* a mechanism known as strong metal-support interaction (SMSI);[44] SMSI has been accounted for stability and selectivity improvement in several reactions by a thin layer of $TiO_x$ species that moves over and partially covers supported metal nanoparticles.[45] The results on the effect of heat treatment are reported in Table 1. Increasing the reduction temperature decreases the activity from 73 for the dried only sample to 50 % for the catalyst heated at 400 °C. However, the stability improves considerably, with the $Au_{50}Pd_{50}/TiO_2$–300 °C and $Au_{50}Pd_{50}/TiO_2$–400 °C catalysts maintain the catalytic activity for 4 consecutive reactions. A small decrease in activity was observed for the $Au_{50}Pd_{50}/TiO_2$–200 catalyst (from 70 to 58 %). MP-AES tests on the final reaction solutions, revealed the absence of Pd, confirming that high temperature treatments help to increase the stability of the catalyst by increasing the metal-support interaction. XPS data (supporting information, Table S5) of the heat-treated catalysts do not suggest significant changes in metal composition with the heat treatment, even though, as mentioned before, these data cannot be considered as a true representation of the real surface composition. The overall loss in activity is probably due to both the suppressed hydrogen chemisorption due to the SMSI and increase in mean particle size with the increased reduction temperature (supporting information, Table S6), with a measured average mean diameter that varies from 2.1 ± 0.6 nm to 5.3 ± 1.2 nm for the $Au_{50}Pd_{50}/TiO_2$ and $Au_{50}Pd_{50}/TiO_2$–400 °C catalysts respectively. On the other hand, the significant improvement in stability may be due to the protective $TiO_x$ surface layer prevent metal sintering phenomena during reaction (Figure 11), and this is confirmed again by TEM analysis (supporting information, Table S6): for high temperature treated catalysts, the nanoparticles dimension changes only slightly (from 5.3 ± 1.2 nm to 5.9 ± 1.3 nm for the $Au_{50}Pd_{50}/TiO_2$–400 catalyst). The high temperature treatments not only influence the activity of the catalysts, but also the selectivity: increasing the reduction temperature, the selectivity towards CAL increases drastically from 40 to 83 % at iso-coversion, with $Au_{50}Pd_{50}/TiO_2$ and $Au_{50}Pd_{50}/TiO_2$–400 respectively. It is well known that high temperature treatments in AuPd alloy systems may cause Pd segregation on the surface of the nanoparticles to form core-shell structures.[46–48] This hypothesis is also consistent with our observations at different Au:Pd ratios, where a Pd rich surface led to higher selectivity towards CAL. XPS analysis cannot

clear out all doubts, since the penetration depth of the X-ray is in the same order of magnitude of the nanoparticle dimensions, and the quantification analysis are good only to evaluate the overall content of the two metals.

The $Au_{50}Pd_{50}/TiO_2$-300 catalyst represents a good compromise between activity, selectivity towards HCAL and stability to reuse, and it is among the most active and selective bimetallic AuPd catalyst reported in literature.[21–24]

## 4. Conclusions

In this study, the catalytic hydrogenation of cinnamaldehyde has been investigated using supported Au-Pd nanoparticles prepared via sol immobilisation method. Systematic studies have been carried out to optimise catalyst properties and reaction conditions. We have shown that the most active bimetallic Au-Pd catalyst is with 1:1 molar ratio. In addition, nature of solvent significantly affects the selectivity for this hydrogenation reaction. When non-polar toluene was used as the solvent higher selectivity of HCAL and HCOH was observed, whereas when polar solvents (ethanol and isopropanol) were used a significant increase in the formation of acetal and PPR was observed. Finally, the effect of heat treatments was studied and by increasing the heat treatment temperature under air and hydrogen we switched off the leaching of Pd observed at lower heat treatment temperatures without significantly affecting the catalytic activity, therefore improving the long-term stability of bimetallic catalysts. The selectivity towards HCAL improved significantly as well, probably due to Pd segregation on the surface of the nanoparticles.

## References


1 Z. Guo, B. Liu, Q. Zhang, W. Deng, Y. Wang and Y. Yang, *Chem. Soc. Rev.*, 2014, **43**, 3480–524.
2 G. C. Bond, *Metal-Catalysed Reactions of Hydrocarbons*, 2005.
3 L. Yin and J. Liebscher, *Chem. Rev.*, 2007, **107**, 133–173.
4 D. I. Enache, J. K. Edwards, P. Landon, B. Solsona-Espriu, A. F. Carley, A. A. Herzing, M. Watanabe, C. J. Kiely, D. W. Knight and G. J. Hutchings, *Science (80-. ).*, 2006, **311**, 362–365.
5 W. Luo, M. Sankar, A. M. Beale, Q. He, C. J. Kiely, P. C. A. Bruijnincx and B. M. Weckhuysen, *Nat. Commun.*, 2015, **6**, 1–10.
6 J. K. Edwards and G. J. Hutchings, *Angew. Chemie Int. Ed.*, 2008, **47**, 9192–9198.
7 P. Mäki-Arvela, J. Hájek, T. Salmi and D. Y. Murzin, *Appl. Catal. A Gen.*, 2005, **292**, 1–49.
8 P. Gallezot and D. Richard, *Selective Hydrogenation of α,β-Unsaturated Aldehydes*, 1998, vol. 40.
9 *Ullmann's Encyclopedia of Industrial Chemistry*, 7th edn., 2014.
10 US 4209643, 1978.
11 US 5632980 A, 1997.
12 E. Bus, R. Prins and J. a. van Bokhoven, *Catal. Commun.*, 2007, **8**, 1397–1402.
13 L. He, J. Ni, L. C. Wang, F. J. Yu, Y. Cao, H. Y. He and K. N. Fan, *Chem. - A Eur. J.*, 2009,

**15**, 11833–11836.
14 C. Milone, C. Crisafulli, R. Ingoglia, L. Schipilliti and S. Galvagno, *Catal. Today*, 2007, **122**, 341–351.
15 H. Shi, N. Xu, D. Zhao and B.-Q. Xu, *Catal. Commun.*, 2008, **9**, 1949–1954.
16 X. Zhang, Y. C. Guo, Z. Cheng Zhang, J. Sen Gao and C. M. Xu, *J. Catal.*, 2012, **292**, 213–226.
17 A. M. R. Galletti, C. Antonetti, A. M. Venezia and G. Giambastiani, *Appl. Catal. A Gen.*, 2010, **386**, 124–131.
18 K. Anderson, S. Cortiñas Fernández, C. Hardacre and P. C. Marr, *Inorg. Chem. Commun.*, 2004, **7**, 73–76.
19 Z. Tian, X. Xiang, L. Xie and F. Li, *Ind. Eng. Chem. Res. 2013*, 2013, **52**, 288−296.
20 S. Fujiwara, N. Takanashi, R. Nishiyabu and Y. Kubo, *Green Chem.*, 2014, 3230–3236.
21 P. Dash, N. A. Dehm and R. W. J. Scott, *J. Mol. Catal. A Chem.*, 2008, **286**, 114–119.
22 T. Szumełda, A. Drelinkiewicz, R. Kosydar and J. Gurgul, *Appl. Catal. A Gen.*, 2014, **487**, 1–15.
23 V. I. Pârvulescu, V. Pârvulescu, U. Endruschat, G. Filoti, F. E. Wagner, C. Kübel and R. Richards, *Chem. - A Eur. J.*, 2006, **12**, 2343–2357.
24 X. Yang, D. Chen, S. Liao, H. Song, Y. Li, Z. Fu and Y. Su, *J. Catal.*, 2012, **291**, 36–43.
25 N. Dimitratos, J. A. Lopez-Sanchez, D. Morgan, A. F. Carley, R. Tiruvalam, C. J. Kiely, D. Bethell and G. J. Hutchings, *Phys. Chem. Chem. Phys.*, 2009, **11**, 5142–5153.
26 Y. Lee and Y. Jeon, *J. korean Phys. Soc.*, 2000, **37**, 451–455.
27 N. Dimitratos, J. A. Lopez-Sanchez, J. M. Anthonykutty, G. Brett, A. F. Carley, R. C. Tiruvalam, A. A. Herzing, C. J. Kiely, D. W. Knight and G. J. Hutchings, *Phys. Chem. Chem. Phys.*, 2009, **11**, 4952.
28 M. Manzoli, A. Chiorino and F. Boccuzzi, *Surf. Sci.*, 2003, **532–535**, 377–382.
29 M. Compagnoni, S. A. Kondrat, C. E. Chan-Thaw, D. J. Morgan, D. Wang, L. Prati, A. Villa, N. Dimitratos and I. Rossetti, *ChemCatChem*, 2016, **8**, 2136–2145.
30 K. Chakarova, M. Mihaylov, S. Ivanova, M. A. Centeno and K. Hadjiivanov, *J. Phys. Chem. C*, 2011, **115**, 21273–21282.
31 T. Tabakova, F. Boccuzzi, M. Manzoli and D. Andreeva, *Appl. Catal. A Gen.*, 2003, **252**, 385–397.
32 T. Lear, R. Marshall, J. A. Lopez-Sanchez, S. D. Jackson, T. M. Klapötke, M. Bäumer, G. Rupprechter, H. J. Freund and D. Lennon, *J. Chem. Phys.*, 2005, **123**, 174706.
33 H. Zhu, Z. Qin, W. Shan, W. Shen and J. Wang, *J. Catal.*, 2004, **225**, 267–277.
34 S. M. Rogers, C. R. A. Catlow, C. E. Chan-Thaw, A. Chutia, N. Jian, R. E. Palmer, M. Perdjon, A. Thetford, N. Dimitratos, A. Villa and P. P. Wells, *ACS Catal.*, 2017, **7**, 2266–2274.
35 A. Villa, N. Dimitratos, C. E. Chan-Thaw, C. Hammond, G. M. Veith, D. Wang, M. Manzoli, L. Prati and G. J. Hutchings, *Chem. Soc. Rev.*, 2016, **45**, 4953–4994.
36 J. H. Carter, S. Althahban, E. Nowicka, S. J. Freakley, D. J. Morgan, P. M. Shah, S. Golunski, C. J. Kiely and G. J. Hutchings, *ACS Catal.*, 2016, **6**, 6623–6633.
37 K. Q. Sun, Y. C. Hong, G. R. Zhang and B. Q. Xu, *ACS Catal.*, 2011, **1**, 1336–1346.
38 W. O. Oduro, N. Cailuo, K. M. K. Yu, H. Yang and S. C. Tsang, *Phys. Chem. Chem. Phys.*, 2011, **13**, 2590–602.
39 S. Mahmoud, A. Hammoudeh, S. Gharaibeh and J. Melsheimer, *J. Mol. Catal. A Chem.*, 2002, **178**, 161–167.
40 L. J. Durndell, C. M. a. Parlett, N. S. Hondow, M. a. Isaacs, K. Wilson and A. F. Lee, *Sci. Rep.*, 2015, **5**, 9425.
41 H. Li, X. Chen, M. Wang and Y. Xu, *Appl. Catal. A Gen.*, 2002, **225**, 117–130.
42 J. P. Breen, R. Burch, J. Gomez-Lopez, K. Griffin and M. Hayes, *Appl. Catal. A Gen.*, 2004, **268**, 267–274.
43 H. Yamada and S. Goto, *J. Chem. Eng. Japan*, 2003, **36**, 586–589.
44 D. D. Eley, H. Pines and P. B. Weisz, *Advances in Catalysis*, Academic Press Inc., 1989.
45 J. C. Matsubu, S. Zhang, L. DeRita, N. S. Marinkovic, J. G. Chen, G. W. Graham, X. Pan and P. Christopher, *Nat. Chem.*, 2016, **9**, 120–127.
46 R. Sharpe, J. Counsell and M. Bowker, *Surf. Sci.*, 2017, **656**, 60–65.
47 A. A. Herzing, A. F. Carley, J. K. Edwards, G. J. Hutchings and C. J. Kiely, *Chem. Mater.*, 2008, **20**, 1492–1501.
48 L. Hilaire, P. Légaré, Y. Holl and G. Maire, *Surf. Sci.*, 1981, **103**, 125–140.

**Table 1.** Catalysts reusability in the CAL hydrogenation. Reaction conditions 90 minutes, 100 °C, 1 $H_2$ bar, catalyst amount 50 mg, CAL 4 mmol, substrate/metal molar ratio 1200:1.

| Catalyst/Catalyst pre-treatment | Run | Mean particle size (nm) | Conv. (%) | Selectivity at 50 % conversion | | | |
|---|---|---|---|---|---|---|---|
| | | | | HCAL | COH | HCOH | PPR |
| $Au_{50}Pd_{50}/TiO_2$ - dried | 1 | 2.1 ± 0.6 | 73 | 40 | 6 | 52 | 2 |
| $Au_{50}Pd_{50}/TiO_2$ - dried | 4 | 3.3 ± 0.9 | 46 | 49 | 5 | 45 | 1 |
| $Au_{50}Pd_{50}/TiO_2$ - 200 °C | 1 | 2.5 ± 0.8 | 70 | 67 | 1 | 31 | 1 |
| $Au_{50}Pd_{50}/TiO_2$ - 200 °C | 4 | 3.4 ± 0.8 | 58 | 62 | 0 | 34 | 3 |
| $Au_{50}Pd_{50}/TiO_2$ - 300 °C | 1 | 3.7 ± 1.0 | 56 | 81 | 0 | 18 | 2 |
| $Au_{50}Pd_{50}/TiO_2$ - 300 °C | 4 | 3.8 ± 0.8 | 55 | 78 | 0 | 21 | 2 |
| $Au_{50}Pd_{50}/TiO_2$ - 400 °C | 1 | 5.3 ± 1.2 | 50 | 83 | 0 | 16 | 1 |
| $Au_{50}Pd_{50}/TiO_2$ - 400 °C | 4 | 5.9 ± 1.3 | 49 | 79 | 0 | 20 | 1 |

**Figure 1.** Cinnamaldehyde hydrogenation pathways.

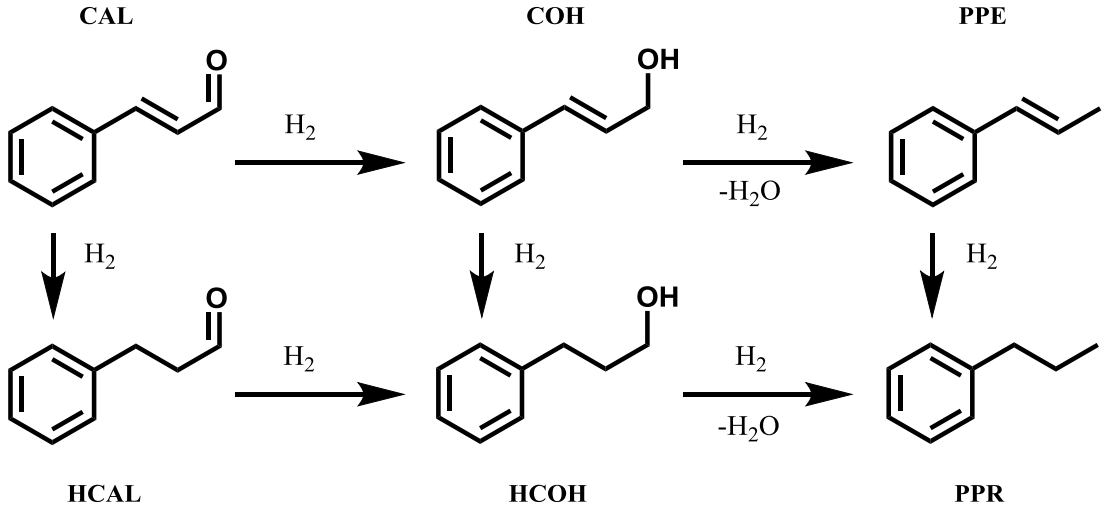

**Figure 2.** Representative TEM images of the fresh catalysts (a) $Au/TiO_2$ (b) $Au_{95}Pd_5/TiO_2$ (c) $Au_{65}Pd_{35}/TiO_2$ (d) $Au_{50}Pd_{50}/TiO_2$ (e) $Au_{35}Pd_{65}/TiO_2$ (f) $Pd/TiO_2$.

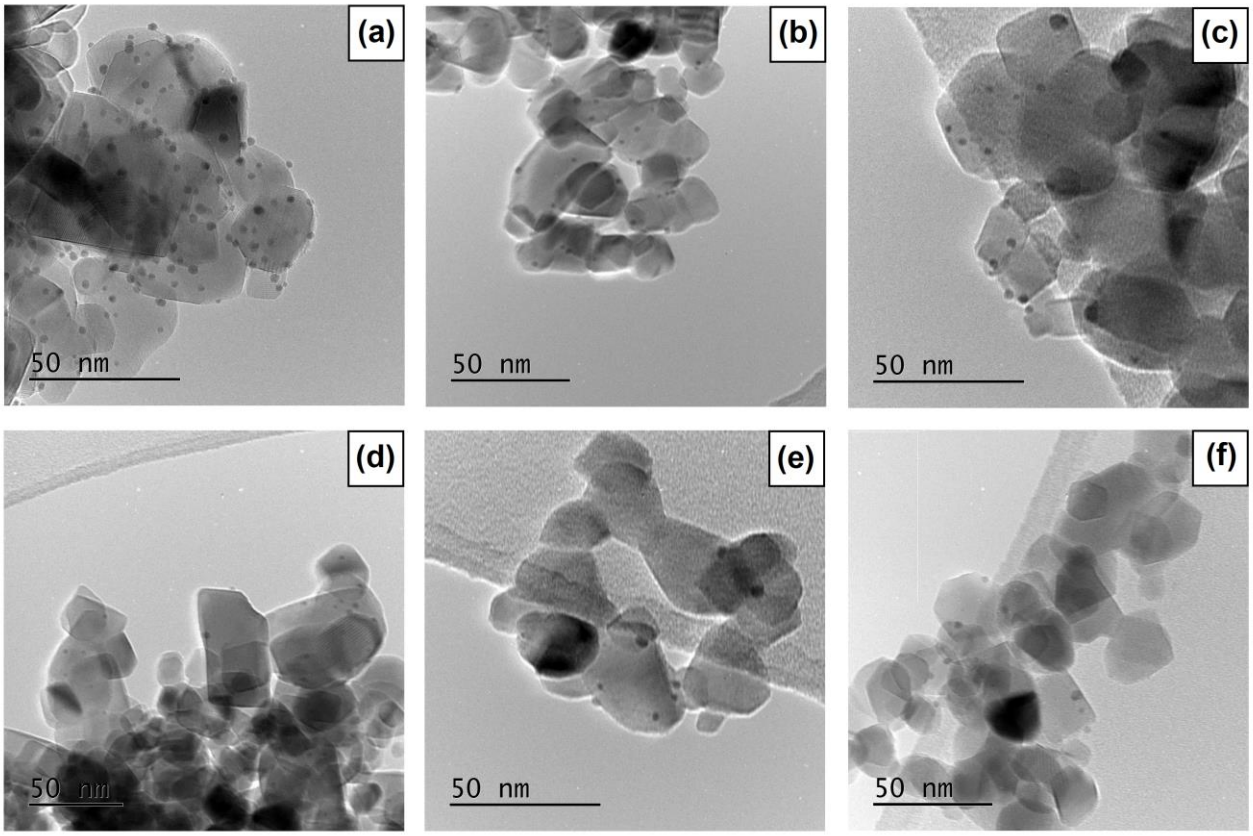

**Figure 3.** Pd (3d) XPS spectra for the $Au_xPd_y/TiO_2$ catalysts: (a) $Pd/TiO_2$ (b) $Au_{35}Pd_{65}/TiO_2$ (c) $Au_{50}Pd_{50}/TiO_2$ (d) $Au_{65}Pd_{35}/TiO_2$ (e) $Au_{95}Pd_5/TiO_2$ (f) $Au/TiO_2$.

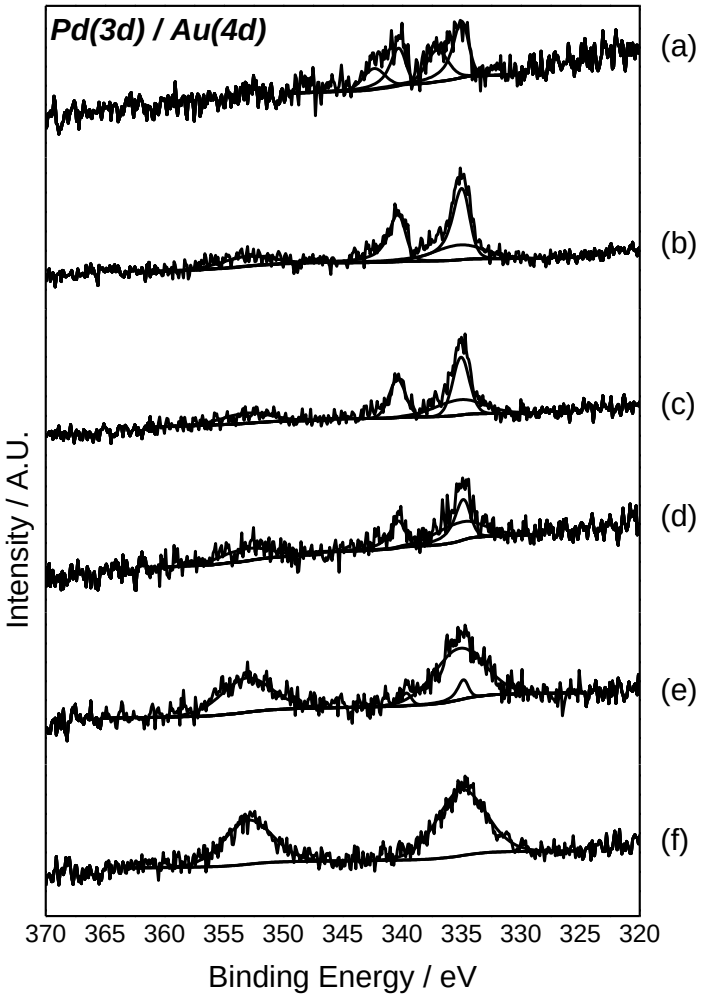

**Figure 4.** CO-DRIFT of (a) $Pd/TiO_2$, (b) $Au_{35}Pd_{65}/TiO_2$, (c) $Au_{50}Pd_{50}/TiO_2$, (d) $Au_{65}Pd_{35}/TiO_2$, (e) $Au_{95}Pd_5/TiO_2$ and (f) $Au/TiO_2$.

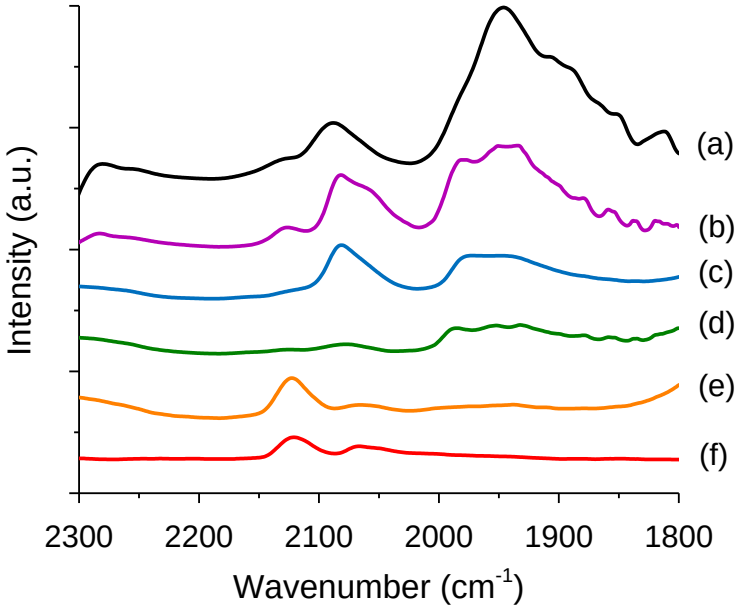

**Figure 5.** Cinnamaldehyde hydrogenation profile. Reaction conditions 100 °C, 1 $H_2$ bar, catalyst amount 50 mg, CAL 4 mmol, substrate/metal molar ratio 1200:1.

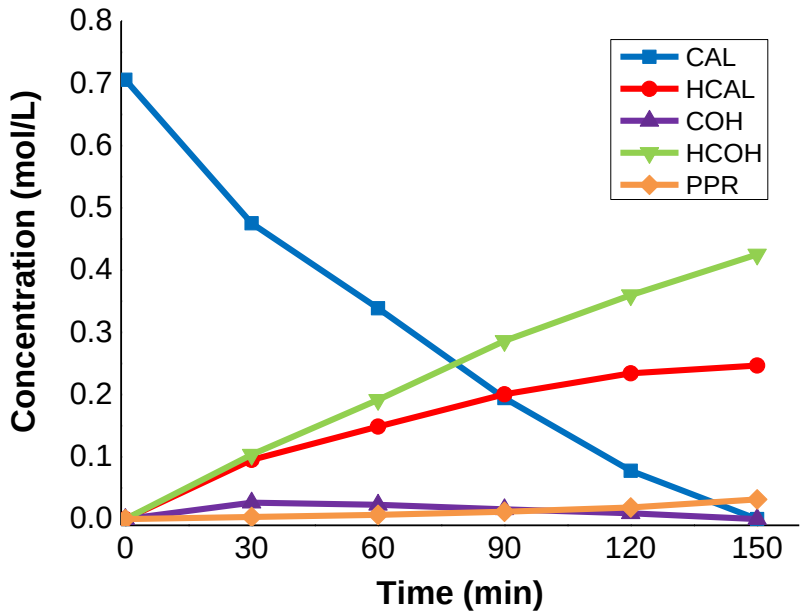

**Figure 6.** Effect of (a) $H_2$ pressure and (b) temperature on the TOF of the reaction. Reaction conditions (a) 100 °C, catalyst amount 50 mg, CAL 4 mmol, (b) 1 $H_2$ bar, catalyst amount 50 mg, CAL 4 mmol.

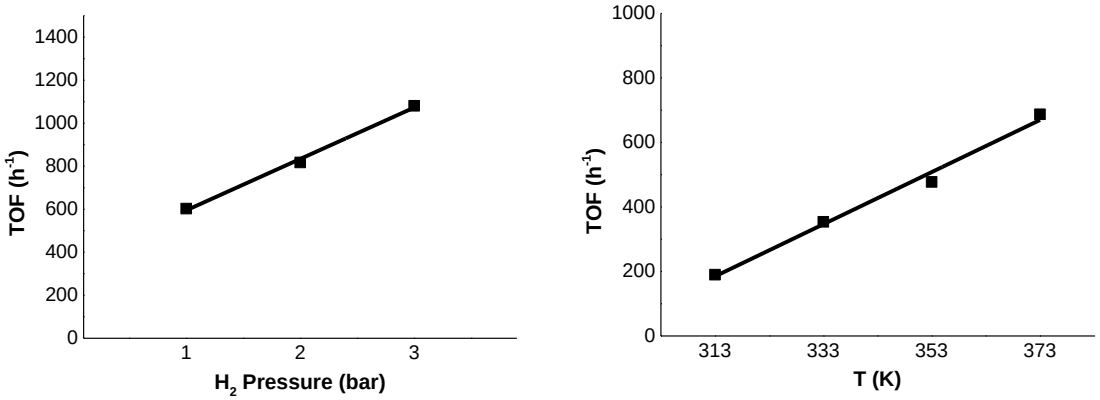

**Figure 7.** Solvent effect in the CAL hydrogenation. Reaction conditions 100 °C, 1 $H_2$ bar, catalyst amount 50 mg, CAL 4 mmol, substrate/metal molar ratio 1200:1.

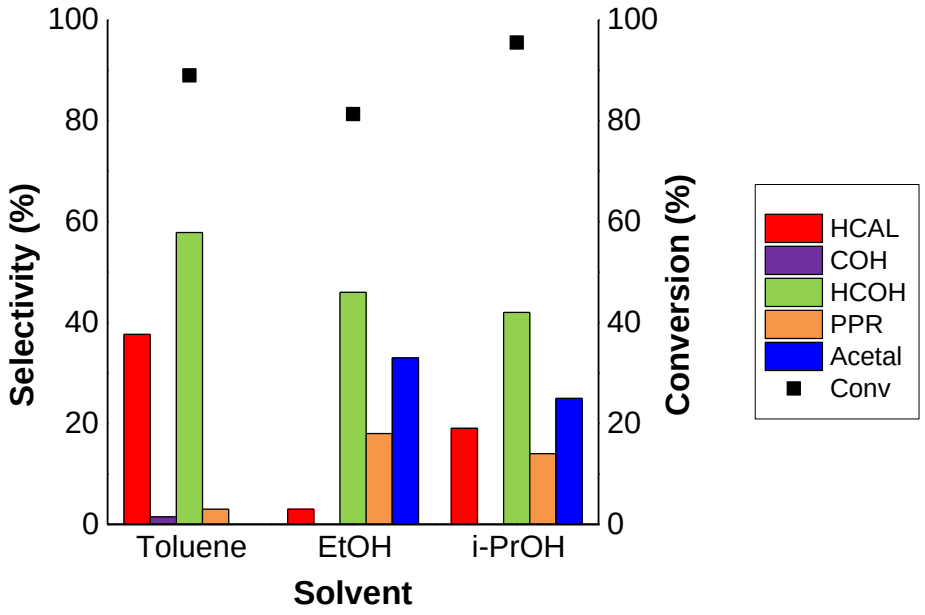

**Figure 8.** Au/Pd ratio effect in the CAL hydrogenation. Reaction conditions 100 °C, 1 $H_2$ bar, catalyst amount 50 mg, CAL 4 mmol, substrate/metal molar ratio 1200:1.

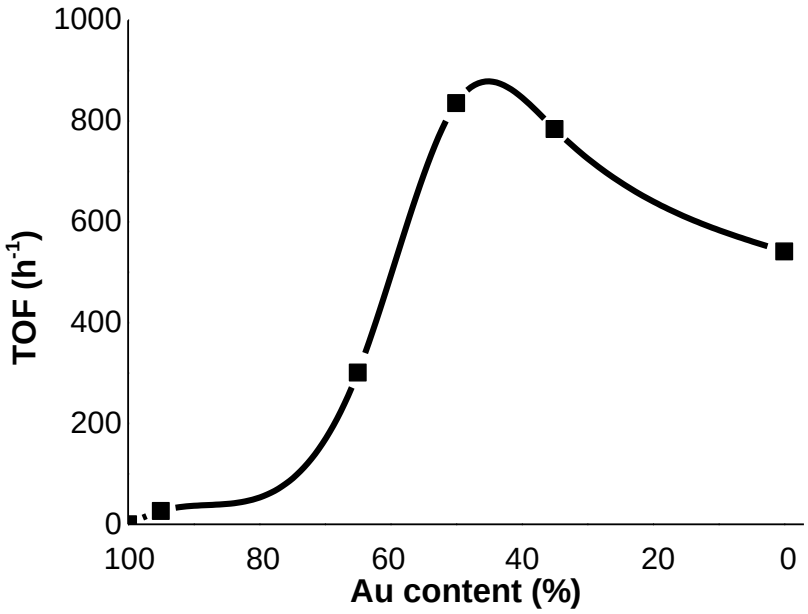

**Figure 9.** Au/Pd molar ratio effect in the CAL hydrogenation. Reaction conditions 100 °C, 1 $H_2$ bar, catalyst amount 50 mg, CAL 4 mmol, substrate/metal molar ratio 1200:1.

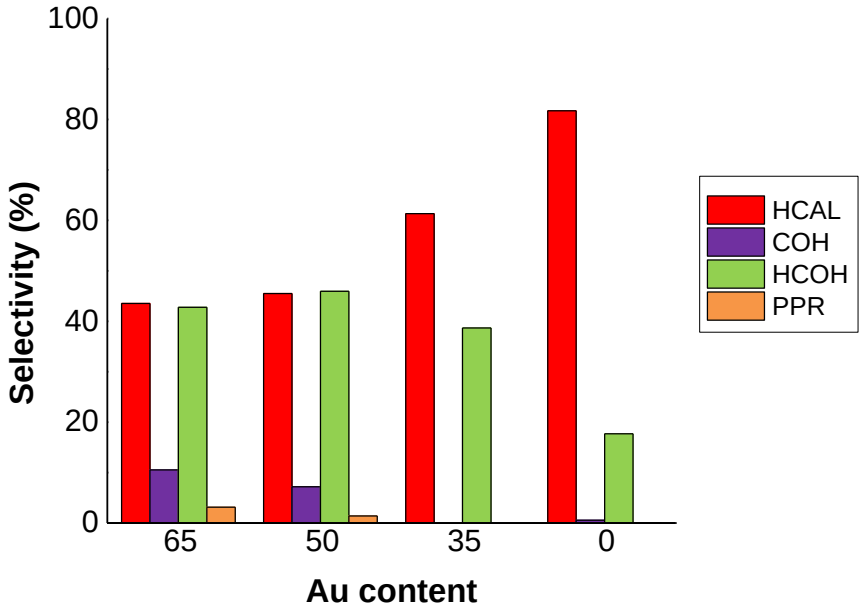

**Figure 10.** Reusability of the $Au_{50}Pd_{50}/TiO_2$ catalyst in the CAL hydrogenation. Reaction conditions 100 °C, 1 $H_2$ bar, catalyst amount 50 mg, CAL 4 mmol, substrate/metal molar ratio 1200:1.

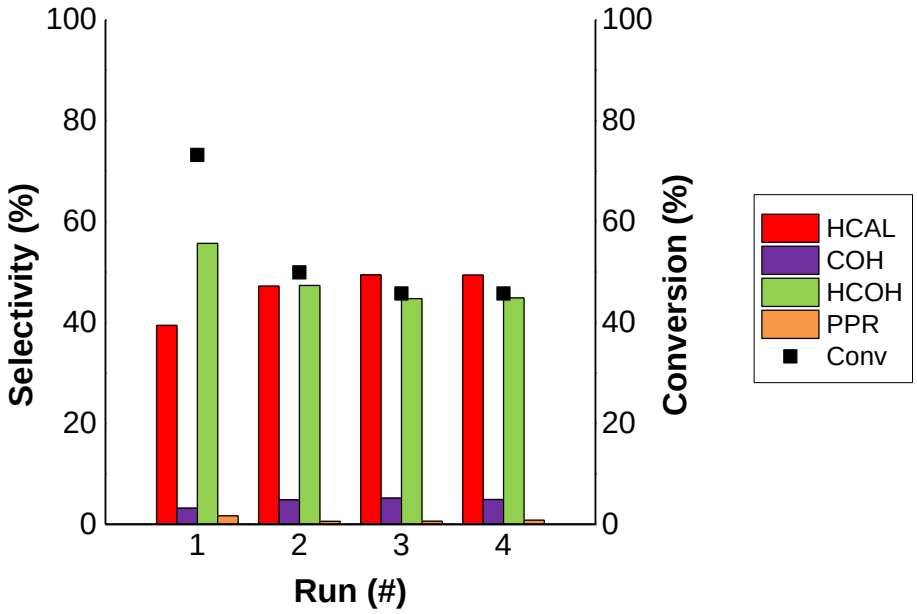

**Figure 11.** TEM evidence of the presence of a $TiO_x$ layer covering the metal NPs.